RSC Advances

PAPER

View Article Online
View Journal | View Issue

Cite this: *RSC Adv.*, 2023, **13**, 28051

A post-sulfonated one-pot synthesized magnetic cellulose nanocomposite for Knoevenagel and Thorpe–Ziegler reactions†

Mostafa Sayed,‡*[ab] Abdelreheem Abdelfatah Saddik, ‡[c] Adel M. Kamal El-Dean,[c] Pedram Fatehi [d] and Ahmed I. A. Soliman *[cde]

The development of biodegradable and active cellulosic-based heterogeneous catalysts for the synthesis of different organic compounds would be attractive in pharmaceutical and petrochemical-related industries. Herein, a post-sulfonated composite of one-pot synthesized magnetite (Fe_3O_4) and cellulose nanocrystals (CNCs) was used as an effective and easily separable heterogeneous catalyst for activating the Knoevenagel and Thorpe–Ziegler reactions. The composite was developed hydrothermally from microcrystalline cellulose (MCC), iron chlorides, urea, and hydrochloric acid at 180 °C for 20 h in a one-pot reaction. After collecting the magnetic CNCs (MCNCs), post-sulfonation was performed using chlorosulfonic acid ($ClSO_3H$) in DMF at room temperature producing sulfonated MCNCs (SMCNCs). The results confirmed the presence of sulfonated Fe_3O_4 and CNCs with a hydrodynamic size of 391 nm (±25). The presence of cellulose was beneficial for preventing Fe_3O_4 oxidation or the formation of agglomerations without requiring the presence of capping agents, organic solvents, or an inert environment. The SMCNC catalyst was applied to activate the Knoevenagel condensation and the Thorpe–Ziegler reaction with determining the optimal reaction conditions. The presence of the SMCNC catalyst facilitated these transformations under green procedures, which enabled us to synthesize a new series of olefins and thienopyridines, and the yields of some isolated olefins and thienopyridines were up to 99% and 95%, respectively. Besides, the catalyst was stable for five cycles without a significant decrease in its reactivity, and the mechanistic routes of both reactions on the SMCNCs were postulated.

Received 10th August 2023
Accepted 5th September 2023

DOI: 10.1039/d3ra05439j

rsc.li/rsc-advances

1. Introduction

Heterogeneous catalysis has emerged as a powerful tool in synthetic organic chemistry because of its facile utilization, effectiveness, reusability, and less hazardous impact.[1,2] In recent years, heterogeneous synthetic strategies have been utilized for synthesizing several biologically or chemically active compounds.[3,4] One of the most significant aspects of organic synthesis is the development of strategies in a green approach. Activating organic reactions using homogenous catalysts suffers from some limitations, such as difficult catalyst recycling, harsh reaction conditions, difficult product isolation, and consumption of large volumes of hazardous organic solvents.[5] In contrast, the use of heterogeneous catalysts would overcome the above-mentioned limitations.

Among the named reactions, Knoevenagel condensation is an essential condensation reaction, which involves a nucleophilic addition of active methylene to carbonyl compounds, which is followed by a dehydration reaction producing α,β-unsaturated molecules *via* forming carbon–carbon double bonds.[6,7] Conventionally, different amines, organometallic catalysts, Lewis acids, such as, $TiCl_4$, $ZnCl_2$, and Al_2O_3, ionic liquids, and amino acids have been efficiently utilized as homogeneous catalysts for Knoevenagel condensation.[7–9] Due to the difficulty in recycling and harsh reaction conditions for homogeneous catalysts, heterogeneous catalysts, such as incorporating zeolites,[10,11] metal–organic frameworks (MOFs),[12,13] ionic liquids, hetero-poly acids,[14] functionalized mesoporous silica,[15] and carbon-based materials,[16,17] have been developed for Knoevenagel condensation. Thorpe–Ziegler cyclization is an intramolecular cyclization of aliphatic

[a]*Department of Chemistry, University of Science and Technology of China, Hefei 230026, China. E-mail: mostafaali@mail.ustc.edu.cn*

[b]*Chemistry Department, Faculty of Science, New Valley University, El-Kharja 72511, Egypt. E-mail: mostafasayed@sci.nvu.edu.eg*

[c]*Chemistry Department, Faculty of Science, Assiut University, Assiut 71516, Egypt. E-mail: ahmed.soliman.38z@science.aun.edu.eg*

[d]*Chemical Engineering Department, Lakehead University, Thunder Bay, ON, P7B5E1, Canada*

[e]*Department of Polymer Science and Engineering, Zhejiang University, Hangzhou, 310027, China*

† Electronic supplementary information (ESI) available: Additional results of TEM, EDX-mapping, thermal properties, FTIR, XRD, and XPS. Analytical data of Knoevenagel and Thorpe–Ziegler products (color, melting point, IR, ^{1}H-NMR, ^{13}C-NMR, and MS). See DOI: https://doi.org/10.1039/d3ra05439j

‡ These authors contributed equally to this manuscript.

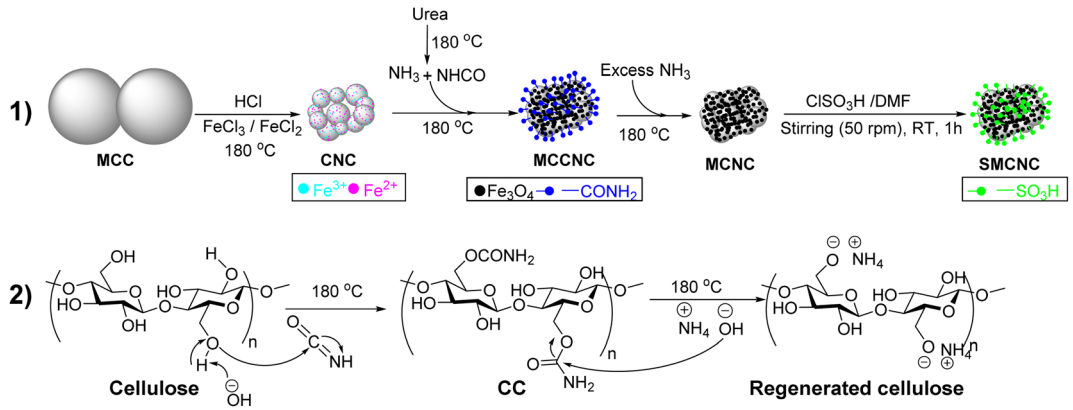

Fig. 1 Schematic illustration of SMCNC development.

carbonitriles into amines, and is useful in synthesizing bioactive heterocycles.[18,19] The cyclization is usually carried out in the presence of organic or inorganic bases, such as sodium ethoxide, sodium hydroxide, or potassium carbonate.[20,21] A previous study revealed that this cyclization process can be catalyzed by a Co_3O_4 nano-catalyst to offer some seleno[2,3-*b*] pyridine/quinoline derivatives[22] with a limited substrate scope. This type of reaction has not been comprehensively studied in the presence of heterogeneous catalysts, which motivated us to develop an easily separable magnetic catalyst for this reaction.

On the other hand, sulfonation reactions are used for activating metal oxides,[23,24] polysaccharides,[25] g-C_3N_4,[26] hydrochar,[27] and zeolites[28] to be used as heterogeneous catalysts for synthesizing hexahydroquinoline,[29] quinazolin-4(3*H*)-one,[25] isoxazole-5-one, spiroindole-fused dihydropyridine,[30] imidazole and pyrimidine derivatives,[28] Knoevenagel condensation,[26,28] Michael addition,[25] and Ritter and multicomponent reactions.[24] Cellulosic-based catalysts have been utilized in organic synthesis,[31] such as Knoevenagel condensation,[32,33] synthesis of isoxazole-5-one derivatives,[34] and Michael addition.[35,36]

Cellulose, which is the most abundant polymer that is biodegradable, has a large surface area, and contains abundant surface hydroxyl groups, which would facilitate its direct chemical modification without requiring tedious or complicated procedures.[37,38] Hence, Shen *et al.* studied the use of water-soluble cellulosic poly(protic ionic liquid) (CPIL) electrolytes as a catalyst for Knoevenagel condensation, with yields up to 90.8%.[39] Sodium carboxymethylcellulose has also been reported as a catalyst for Knoevenagel condensation in 98% yield under solvent-free conditions and at room temperature.[40] Herein, magnetic cellulose nanocrystals, MCNCs, were hydrothermally synthesized in a one-pot reaction and then post-sulfonated using chlorosulfonic acid (CSA), producing sulfonated MCNCs (SMCNCs), as illustrated in Fig. 1. The use of cellulose would enable the hydrothermal development of Fe_3O_4 in a one-pot reaction without requiring organic solvents such as ethylene glycol or a surfactant to prevent agglomeration.[41,42] Besides, versatile chemical modifications of cellulose were reported and one of these modifications was sulfonation, which can be performed at RT from $ClSO_3H$/DMF in a short-time one-step reaction without requiring large amounts of $ClSO_3H$.[43] The presence of SO_3H components in the SMCNCs would catalyze the synthesis of different organic compounds as mentioned above, and containing Fe_3O_4 would facilitate the separation of the catalyst from the reaction mixture by applying an external magnetic field. Therefore, the SMCNC catalyst was applied in Knoevenagel condensation and Thorpe–Ziegler cyclization for the first time, to the best of our knowledge. The optimization and scope of both reactions were investigated with concluding the mechanistic routes. Also, the recyclability of the catalyst was investigated based on the stability and efficiency of the catalyst during several reaction cycles.

2. Results and discussion

2.1. Hydrothermal development of the SMCNCs

The XRD spectra of MCC, Fe_3O_4, and SMCNCs are illustrated in Fig. 2. The diffraction peaks at 2θ of 14.9°, 16.6°, 20.7°, 22.6°, and 34.5° are attributed to the ($1\bar{1}0$), (110), (021), (200), and (004) planes of MCC, respectively.[44,45] The diffraction peaks at 18.3°, 30.1°, 35.4°, 37.1°, 43.1°, 53.5°, 57.3°, and 62.7° were assigned to the (111), (220), (311), (222), (400), (422), (511), and (440) planes of Fe_3O_4, respectively.[46,47] The XRD spectrum of the SMCNCs shows the diffraction peaks of both MCC and Fe_3O_4. The CrI values of MCC and the SMCNCs, which were calculated from eqn (1) using the intensity under the peak at 22.6° (I_{200}) and the intensity under the amorphous peak at 18.6° ($I_{amorphous}$) as illustrated in Fig. S1,† were 89.6% and 76.6%, and the decrease in CrI could be ascribed to the partial destruction of the cellulose crystallinity during the hydrothermal and post-sulfonation treatments.[48–50]

$$\mathrm{CrI}(\%) = \frac{I_{200} - I_{\mathrm{amorphous}}}{I_{200}} \quad (1)$$

The FTIR spectra of Fe_3O_4, MCC, and the SMCNCs are shown in Fig. 3. The absorption bands at 895 cm^{-1}, 1313 cm^{-1}, 1425 cm^{-1}, 2895 cm^{-1}, and 3332 cm^{-1} were assigned to the δ(C–H), δ(O–H), δ(CH_2), ν(CH_2) and ν(O–H) vibrations of MCC,

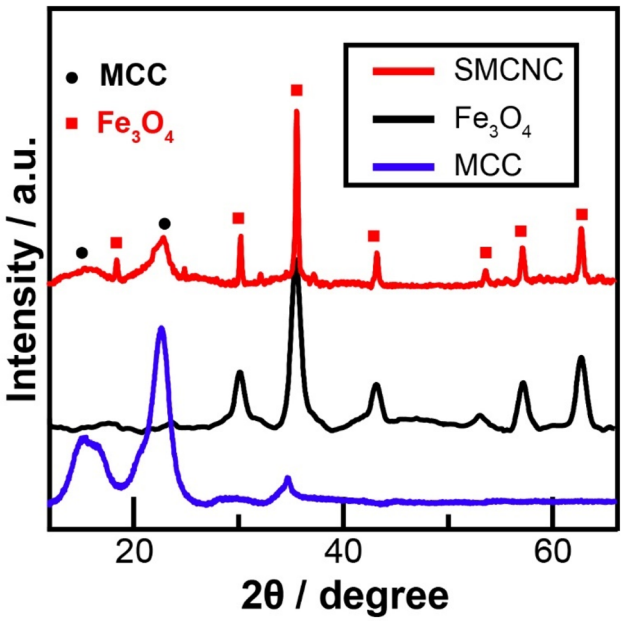

Fig. 2 XRD spectra of the Fe_3O_4, MCC, and SMCNC samples.

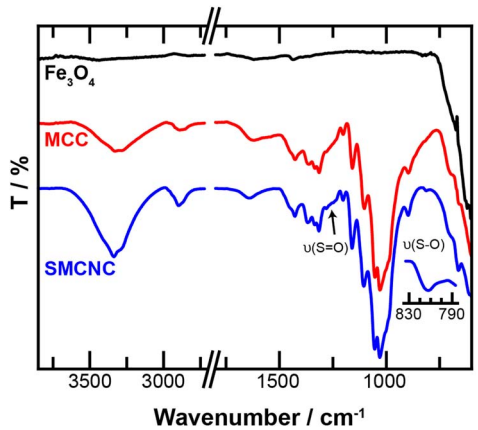

Fig. 3 ATR-FTIR spectra of the Fe_3O_4, MCC, and SMCNC samples.

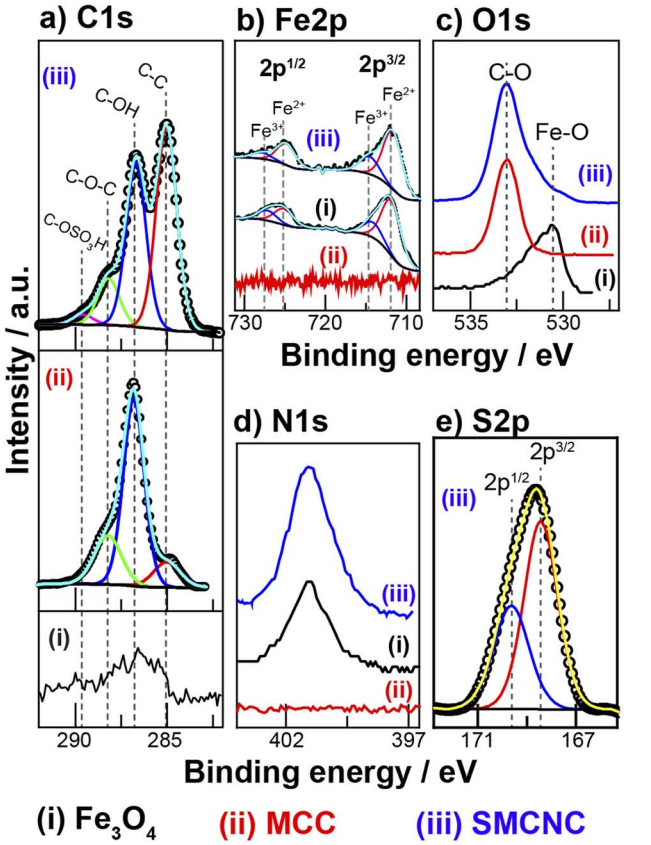

Fig. 4 XPS (a) C 1s, (b) Fe 2p, (c) O 1s, (d) N 1s, and (e) S 2p spectra of the Fe_3O_4, MCC and SMCNC samples.

respectively. The FTIR spectrum of the SMCNCs exhibits absorption bands attributed to the C–H, C–O, and O–H stretching and bending vibrations of cellulose, which confirms the presence of crystalline cellulosic components under the hydrothermal and post-sulfonation treatments. Absorption bands attributed to the ν(S=O) and ν(S–O) of the SO_3H groups after post-sulfonation were observed at 1237 cm^{-1} and 812 cm^{-1}, respectively.[43,51,52]

The XPS C 1s, Fe 2p, O 1s, N 1s, and S 2p spectra of Fe_3O_4, MCC, and the SMCNCs are illustrated in Fig. 4. Three deconvoluted peaks were observed in the C 1s spectrum of MCC at 285.1 eV, 286.7 eV, and 288.0 eV, and these peaks were assigned to C–C, C–O–H, and C–O–C, respectively. The carbon content of the Fe_3O_4 sample, which could be assigned to the C–N and C=O components, originated from the hydrothermal decomposition of urea. The carbon components of the SMCNCs were deconvoluted into C–C, C–OH, C–O–C, and C–OSO_3H components at 285.0 1 eV, 286.7 eV, 288.0 eV, and 289.6 eV, respectively. The Fe 2p spectra show the presence of iron components in the Fe_3O_4 and SMCNC samples. Four peaks observed at 710.7 eV, 713.6 eV, 724.1 eV, and 727.2 eV were assigned to the Fe^{2+} $2p^{3/2}$, Fe^{3+} $2p^{3/2}$, Fe^{2+} $2p^{1/2}$ and Fe^{3+} $2p^{1/2}$, respectively.[53,54] The O 1s spectrum of MCC shows a peak at 532.8 eV, which is assigned to the O–C component. The oxygen content of Fe_3O_4 was ascribed to the O–Fe component, which is allocated at 530.6 eV.[53,55] The N 1s spectra show the presence of nitrogen components at 401.1 eV in both the Fe_3O_4 and SMCNC samples.[56,57] The presence of SO_3H components can also be indicated from the XPS S 2p spectrum, which is deconvoluted into S $2p^{3/2}$ and S $2p^{1/2}$ peaks at 168.5 eV and 169.7 eV, respectively.[26,58] The atomic percentage of sulfur in the composite was estimated as 1.1%.

The hydrodynamic diameter of MCC decreased after SMCNC development from 51 000 nm to 391 nm (±25), which illustrates that the hydrothermal treatment of MCC in the presence of $FeCl_3$, $FeCl_2$, urea, and HCl at 180 °C followed by a post-sulfonation process can convert the MCC into SMCNCs. Previously, one-pot synthesis of CNCs was reported through hydrothermal treatment in the presence of mineral acids and inorganic chlorides.[44,59] The zeta potential values of the SMCNCs were found to be +13.7 mV (±3.5), −2.94 mV (±1.1),

and −11.39 mV (±3.8) at the pH values of 3, 7, and 10, respectively. The changes in zeta potential at different pHs could be ascribed to the chemical changes in the SO_3H groups, nitrogen components, and cellulosic moieties.

Fig. 5 shows the TEM images of the SMCNCs, where Fe_3O_4 nanoparticles were observed on the CNCs without the presence of agglomerations. The presence of cellulose suppressed the formation of aggregations during the hydrothermal process without requiring capping agents.[41,42] The cubic and octahedral morphologies of Fe_3O_4 were detectable, and the lattice fringe spacings of ~0.30 and ~0.26 nm could be ascribed to the (220) and (311) planes of Fe_3O_4, respectively.[60] The EDX mapping of carbon, iron, and sulfur is illustrated in Fig. S2,† where the iron components were distributed on the CNC components, confirming the deposition of Fe_3O_4 on the CNCs. The EDX-mapping of sulfur illustrates that sulfur was distributed on both the CNCs and Fe_3O_4, indicating the occurrence of sulfonation on both the CNC and Fe_3O_4 components, which agreed with the previous reports.[30,34]

The thermal gravimetrical analysis (TGA) and differential thermal analysis (DTA) curves of the SMCNCs are illustrated in Fig. 6. The weight loss at <185 °C, which was 6%, was attributed to the removal of SO_3H and adsorbed moisture. In the range of 185 °C to 455 °C, the significant weight loss (38%) was ascribed to cellulose degradation and the transformation of Fe_3O_4 to Fe_2O_3.[61,62] The decrease in the thermal stability of the SMCNCs could be ascribed to the decrease in the cellulose crystallinity because of the post-sulfonation.[63–65]

Based on the given results and as illustrated in Fig. 1, the hydrothermal treatment of MCC in the presence of $FeCl_3$, $FeCl_2$, urea, and HCl at 180 °C for 20 h would produce a composite of Fe_3O_4 and CNCs as indicated by the XRD patterns, TEM measurements, and EDX-mapping of these components. The XPS spectra illustrate the elements of both Fe_3O_4 and CNCs. The acid hydrolysis in the presence of $FeCl_3$ and $FeCl_2$ reduced the size of the MCC to CNCs.[44,59,66] The thermal decomposition of urea produced ammonia and isocyanic acid, which converted the $FeCl_3$ and $FeCl_2$ into Fe_3O_4 and cellulose into cellulose carbamate, entitled as MCCNCs.[67–69] Under higher temperatures, the presence of excess ammonia would facilitate the cellulose regeneration from the cellulose carbamate producing MCNCs, which could explain the absence of FTIR adsorption bands that could be assigned to ν(C═O) at >1700 cm^{-1}.[45,70] The post-sulfonation of the synthesized composite using $ClSO_3H$ would functionalize the surface of both the CNCs and Fe_3O_4 by SO_3H, as indicated by the XPS S 2p spectrum, EDX-mapping of sulfur and decrease of thermal stability. The insertion of these sulfonic groups influenced the thermal stability and zeta potential of the developed SMCNCs.

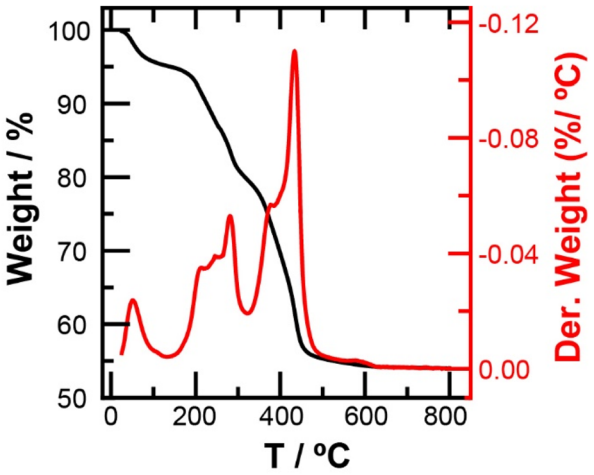

Fig. 6 TGA and DTA of SMCNC.

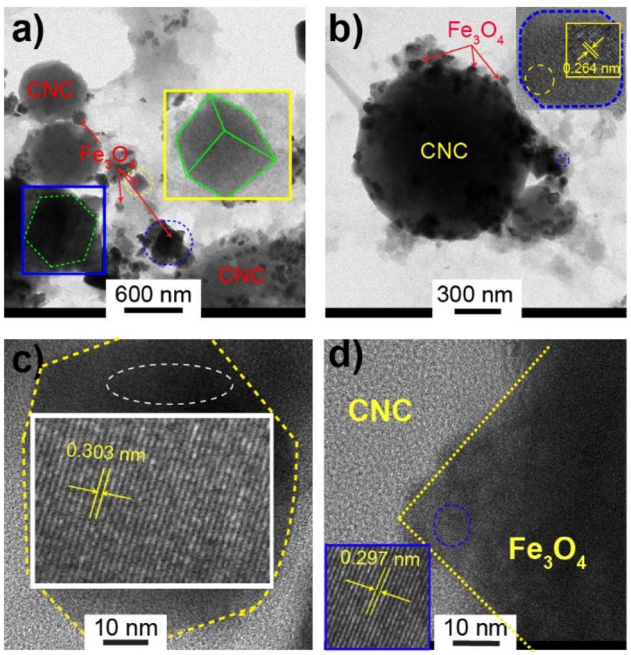

Fig. 5 (a and b) TEM and (c and d) HR-TEM images of the SMCNCs.

2.2. Knoevenagel condensation

2.2.1. The optimal conditions. To determine the optimal reaction conditions, the reactions were studied using benzaldehyde **1a** (2 mmol), and malononitrile **2a** (3 mmol) in polar and non-polar solvents at different temperatures as presented in Table 1. Primarily, when the reaction was conducted in ethanol at reflux in the absence of the SMCNC catalyst for 1 h, only trace amounts of the product were detected by TLC with a slight substrate conversion (entry 1). The reaction was conventionally realized in ethanol using piperidine as a homogeneous catalyst and product **3a** was collected in 90% yield after 30 min (entry 2). To explore the catalytic efficiency of the SMCNCs, the reaction was performed in refluxed ethanol in the presence of an SMCNC (10% wt.) catalyst for 1 h, and fortunately, the product was furnished in 90% yield (entry 3). To study the temperature effect, the reaction was conducted at ambient temperature for 1 h in ethanol and the yield increased to 95% (entry 4). The reaction yield was still unchanged even if the reaction time was shortened to 30 min (entry 5). The optimization of the solvent was also investigated showing that water

Table 1 Procedure optimization of the Knoevenagel reaction[a]

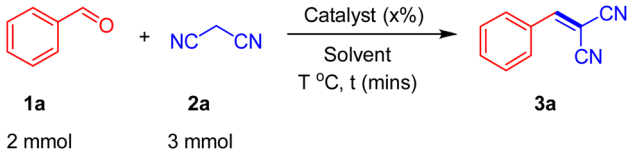

Entry	Catalyst	Cat. load[b] (%)	Solvent	T (°C)	t (min)	Yield[c] (%)
1	—	—	EtOH	80	60	Trace
2	Piperidine	10	EtOH	80	30	90
3	SMCNC	10	EtOH	80	60	90
4	SMCNC	10	EtOH	r.t	60	95
5	SMCNC	10	EtOH	r.t	30	95
6	SMCNC	10	Hexane	r.t	30	60
7	SMCNC	10	Tol	r.t	30	50
8	SMCNC	10	DMF	r.t	30	90
9	SMCNC	10	H_2O	r.t	30	97
10	SMCNC	10	H_2O	80	30	85
11	SMCNC	10	Neat	r.t	30	92
12	SMCNC	20	H_2O	r.t	30	98
13	SMCNC	15	H_2O	r.t	30	97
14	SMCNC	5	H_2O	r.t	30	80

[a] Reaction conditions: **1a** (2.0 mmol), **2a** (3.0 mmol), solvent (5 mL). [b] The catalyst percent was calculated relative to the weight of the benzaldehyde substrate. [c] Isolated yield.

was the optimal solvent for Knoevenagel condensation (entries 6–9), while the non-polar solvents, such as toluene or hexane, provided **3a** in a decreased yield. These results showed a considerable positive effect of the polar solvents on the catalytic activity of the developed catalyst over the non-polar solvents. In light of Gutmann's Donor Number (DN), Acceptor Number (AN), and dielectric constant of the used solvents listed in Table S1.† Boosting of the isolated yield in the presence of polar solvents might be attributed to their Lewis basicity,[71–73] alteration of the catalyst adsorption/desorption behavior,[74,75] and formation of hydrogen bonds between the catalyst and the reaction substrates.[72–74] Another merit of polar solvent usage is the better and homogenous dispersion of the catalyst and other reactants during vigorous stirring conditions.[73,76] Also, the presence of the SO_3H group in SMCNC opens the opportunity for hydrogen bonding with the polar solvents of EtOH, DMF, and H_2O.[77,78] Consequently, these polar solvents are expected to act as reactants in the reaction mechanism by solvation and proton transfer effects, and their reactivities are determined by their strength as a donor or acceptor.[71,72] If the reaction proceeds in neat conditions, product **3a** is produced with a yield of 92% (entry 11). Moreover, the load of the SMCNC catalyst was studied by trying different loads of the catalyst, including 20%, 15%, and 5% wt. (entries 12–14), and the results showed that the high catalyst loads did not show a significant influence on the yield, but when the load was reduced to 5%, the reaction yield decreased to 80%, which would indicate that 10% wt. catalyst load was the optimal load for the reaction.

2.2.2. The reaction scope. After the reaction conditions were optimized, the Knoevenagel reaction was examined using different aromatic and heterocyclic aldehydes (**1a–1n**) with malononitrile **2a** and ethyl cyanoacetate **2b** as the active hydrogen species. As demonstrated in Scheme 1, a green approach utilizing water for the synthesis of α,β-unsaturated esters, and nitriles by Knoevenagel condensation was effectively developed. Using a wide range of aromatic and heterocyclic aldehydes, the Knoevenagel reaction smoothly delivered an interesting class of α,β-unsaturated derivatives under the optimized conditions. Aromatic aldehydes bearing both electron-deficient substituents and electron-rich substituents were successfully reacted with malononitrile **2a** and ethyl cyanoacetate **2b**. Aldehydes with electron-withdrawing groups exhibited a high activity over the aldehydes with the electron-donating ones, for example, *p*-nitrobenzaldehyde reacted with both malononitrile and ethyl cyanoacetate, and the **3ba** and **3bb** products were obtained in 99% and 97% yields, respectively, whereas the reaction of *o*-nitrobenzaldehyde with malononitrile and ethyl cyanoacetate under the optimized conditions delivered the products **3ca** and **3cb** in 97% and 95% yields, respectively. Also, *p*-chlorobenzaldehyde and *m*-chlorobenzaldehyde were explored in this investigation with both malononitrile and ethyl cyanoacetate to produce the corresponding Knoevenagel products **3da**, **3ea**, **3db**, and **3eb** with the yields of 98%, 95%, 95%, and 96%, respectively. The presence of electron withdrawing substituents on the benzene ring facilitated the polarization of the formyl group of the aldehydes, which in turn enabled the coordination with iron metal. Aldehydes with electron-rich substituents, such as methyl or methoxy groups, were efficiently examined in our strategy, and *p*-tolylaldehyde was reacted with malononitrile and ethyl cyanoacetate under the optimized conditions to synthesize the **3fa** and **3fb** products in 93% and 94% yields, respectively. Also, *o*- and *m*-anisidine have been tested with malononitrile to generate **3ga** and **3ha** in yields of 93% and 95%, respectively, while with ethyl cyanoacetate, the reaction produced **3gb** and **3hb** in 93% and 92% yield, respectively. Interestingly, cinnamaldehyde was found to be a potent substrate in this transformation with both malononitrile and ethyl cyanoacetate delivering the products **3ja** and **3jb** in excellent yields of 97% and 98, respectively. Remarkably, 1-naphthaldehyde produced **3ka** and **3kb** in 95% and 96% yields, respectively. In addition, heterocyclic carbaldehydes, such as indole-3-carbaldehyde and thiophene-3-carbaldehyde, were nicely observed as suitable substrates for this process with malononitrile yielding products **3la** and **3ma** with yields of 99% and 98%, respectively. Finally, an aldehyde with three fused benzene rings was successfully reacted with ethyl cyanoacetate under the optimized conditions to produce **3lb** in 85% yield.

2.3. Thorpe–Ziegler condensation

2.3.1. The optimal conditions. The Thorpe–Ziegler reaction is a self-condensation reaction of aliphatic nitriles catalyzed by a base to produce enamines, and it is considered an important reaction in organic synthesis because it can provide a wide class

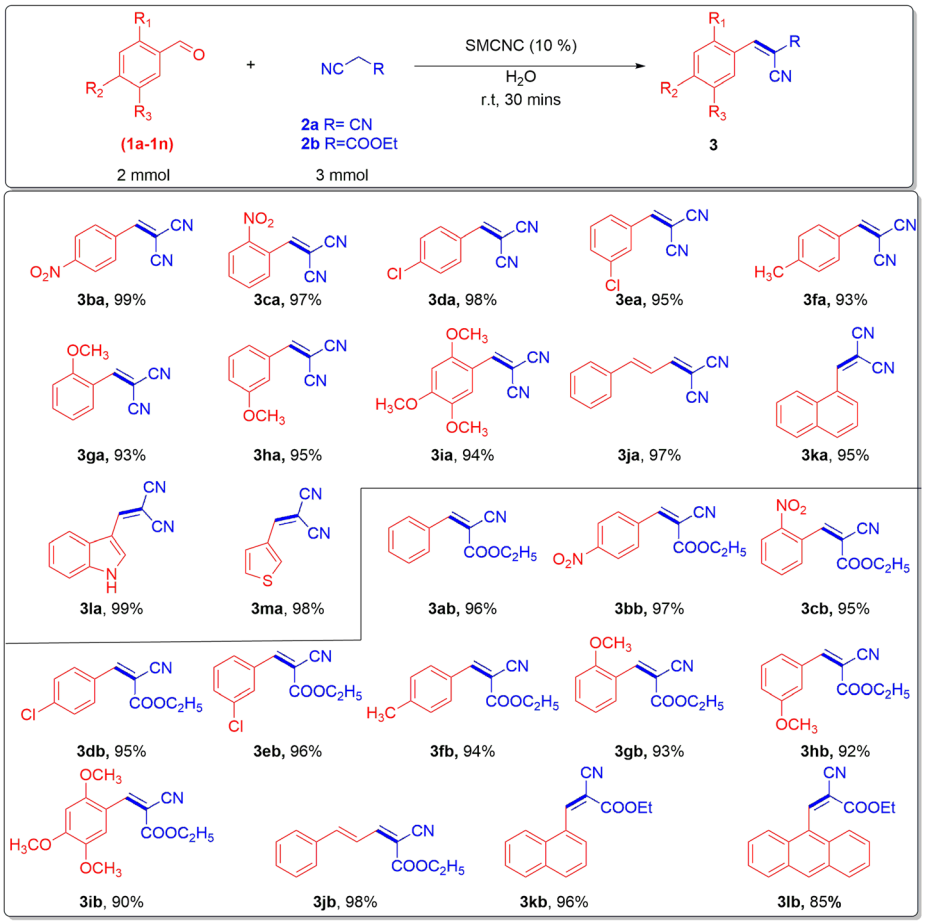

Scheme 1 The substrate scope of aromatic aldehydes with malononitrile and ethyl cyanoacetate.

Table 2 Optimization of the Thorpe–Ziegler reaction[a]

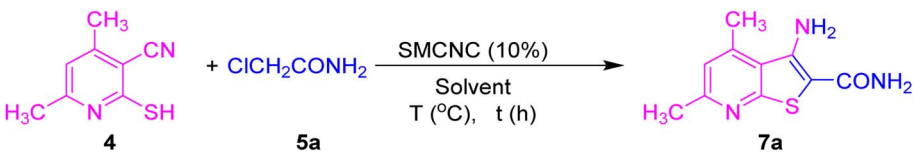

Entry	Catalyst[b] (10%)	T (°C)	t (h)	Solvent	Yield[c] (%)
1	EtONa	Reflux	4	EtOH	90
2	Piperidine	Reflux	4	EtOH	50
3	K_2CO_3	Reflux	4	EtOH	80
4	—	Reflux	4	EtOH	N.D
5	SMCNC	Reflux	2	H_2O	Traces
6	SMCNC	r.t	2	H_2O	Traces
7	SMCNC	Reflux	1	DMF	40
8	SMCNC	Reflux	2	Toluene	Traces
9	SMCNC	Reflux	2	EtOH	90
10	SMCNC	r.t	2	EtOH	60
11	SMCNC	Reflux	3	EtOH	90
12	SMCNC[d]	Reflux	2	EtOH	90

[a] Reaction conditions: **4** (2.0 mmol), **5** (3.0 mmol), solvent (5 mL). [b] The catalyst percent was calculated based on the amount of substrate **4**. [c] Isolated yield of product **7a**. [d] 20% catalyst loading was used.

of biofunctionalized heterocyclic compounds that serve as dominant intermediates for the synthesis of many natural products and pharmaceutical drugs. Inspired by the outstanding catalytic activity of SMCNCs and considering their advantages as an easily separable and recyclable catalyst, with a shortened reaction time, we used this catalyst for both alkylation and Thorpe–Ziegler reactions, which have not been reported before, to the best of our knowledge. The conditions were optimized as illustrated in Table 2. To start with, 4,6-dimethyl-2-thioxo-1,2-dihydropyridine-3-carbonitrile **4** and chloroacetamide **5a** were selected as substrates for this approach, and the process was initially investigated in sodium ethoxide as an organic base and ethanol as a solvent. The cyclized product **7a** was collected in 90% yield after 2 h of refluxing (entry 1). After that, the reaction was attempted under the same conditions except for the catalyst, where both piperidine, as an organic base, and potassium carbonate, as an inorganic base, were examined, and the product was obtained in 50% and 80% yield, respectively. These results suggested that sodium ethoxide was the best homogeneous catalyst for this reaction. Notably, **7a** was not detected in the absence of the catalyst (entry 4) revealing that the base was crucial for this reaction. Trying the above-mentioned optimized conditions of Knoevenagel condensation using the SMCNCs in water for 2 h induced only a trace amount of the product (entries 5 and 6). Optimization of the solvent (entries 7–9) revealed that ethanol was the optimal solvent, where the product was successfully separated in 90% yield after a 2 h reaction time, which suggested that the reaction could be catalyzed by our developed catalyst. The results of solvent optimization showed that polar solvents are crucial for this reaction, and the use of polar solvents gave better dispersion and homogenous mixing of the reaction mixture, as previously mentioned. High-temperature reaction conditions are necessary to dissolve the reactants. Unfortunately, when the reaction was conducted at ambient temperature, the product was only delivered in a 60% yield (entry 10); however, increasing the reaction time to 3 h at reflux temperature did not result in an improved yield (entry 11). Finally, increasing the catalyst loading to 20% led to the same yield as the 10% catalyst loading (entry 12).

2.3.2. The reaction scope. The reaction scope was further explored using compound **4** and different α-halogenated carbonyl compounds **5** under the optimal conditions. As shown in Scheme 2, conducting the reaction in ethanol at reflux temperature for only 1 h in the presence of SMCNCs (10%) produced the intermediate **6** (*S*-alkylated product), which can be transformed into the cyclized thienopyridine product **7** by stirring in ethanol using the SMCNCs (10%) for an additional 1 h. Hence, the SMCNC catalyst effectively catalyzed both the alkylation reaction of thiol compounds and intramolecular Thorpe–Ziegler cyclization, and the scope of both reactions was investigated offering a different class of *S*-alkylated pyridines (**6a–6i**), and amino-functionalized thienopyridine compounds (**7a–7i**).

From the optimization of the procedure, it was found that chloroacetamide **5a** can be reacted with compound **4** in ethanol under reflux for 1 h using 10% SMCNCs to produce compound **6a** in 90% yield, and then **6a** can be cyclized in ethanol using the recovered catalyst for 30 min to deliver compound **7a**. Moreover, ethyl chloroacetate **5b** was applied in this reaction under the optimized conditions to get **6b** in 92% yield, which was further

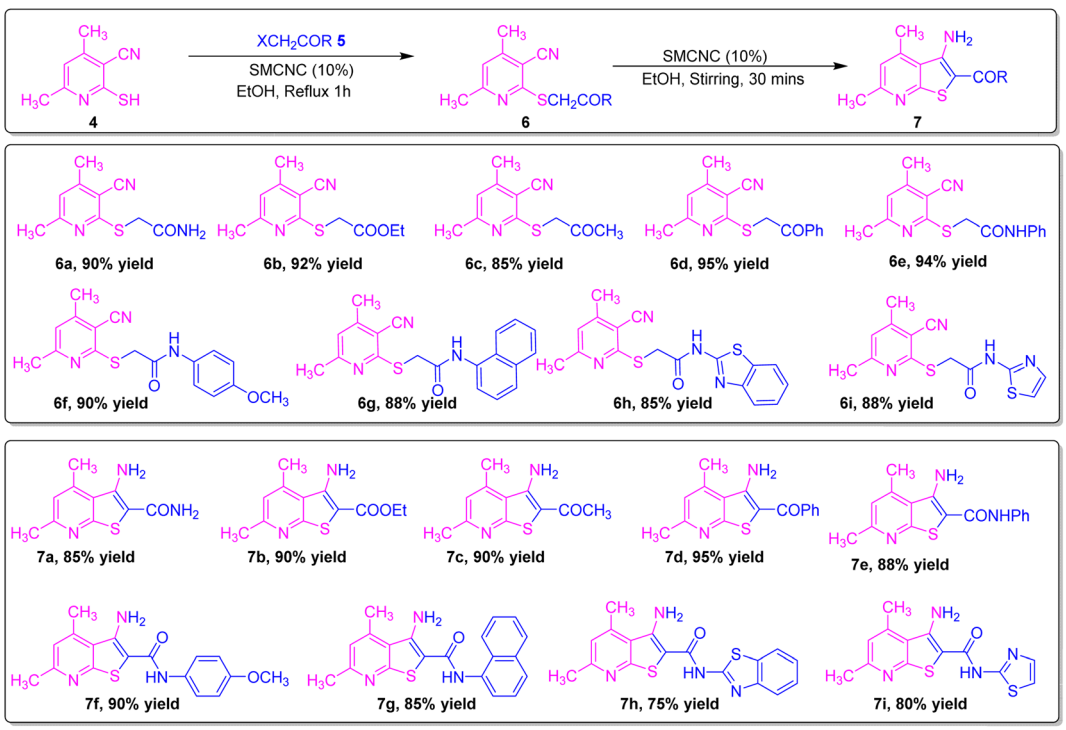

Scheme 2 The substrate scope of compound **4** with different halogenated carbonyl compounds.

cyclized in the second step to produce amino ester functionalized thienopyridine **7b** in 90% yield. Also, chloroacetone **5c** and phenacyl bromide **5d** were successfully examined in this strategy for the reaction with dimethylpyridine, delivering derivatives **6c** and **6d** in 85% and 95% yields, respectively, which were further subjected to cyclization reactions providing **7c** and **7d** in 90% and 95% yields, respectively. Phenacyl bromide exhibited higher activity over chloroacetone, which may be attributed to the facilitation of the nucleophilic substitution by the larger size of bromine. Furthermore, chloroacetanilide derivatives **5e** and **5f** were efficiently explored as halogenated carbonyl compounds to produce *S*-alkylated products **6e** and **6f** in 94% and 90% yields, respectively. The methoxy substituent in **6f** lowered the yield due to its electron-donating nature, and then the intramolecular cyclization of the latter compounds generated **7e** and **7f** in 88% and 90% yields. Fused chloronaphthanilide derivative **5g** was also investigated in this conversion, and product **6g** was delivered in 88% yield, which was subjected to further transformation to **7g** in 85% yield. The heterocyclic derivatives benzothiazole **5h** and thiazole **5i** were tolerated to afford products **6h** and **6i** in 85% and 88% yields, respectively, and **7h** and **7i** in 75% and 80% yields, respectively.

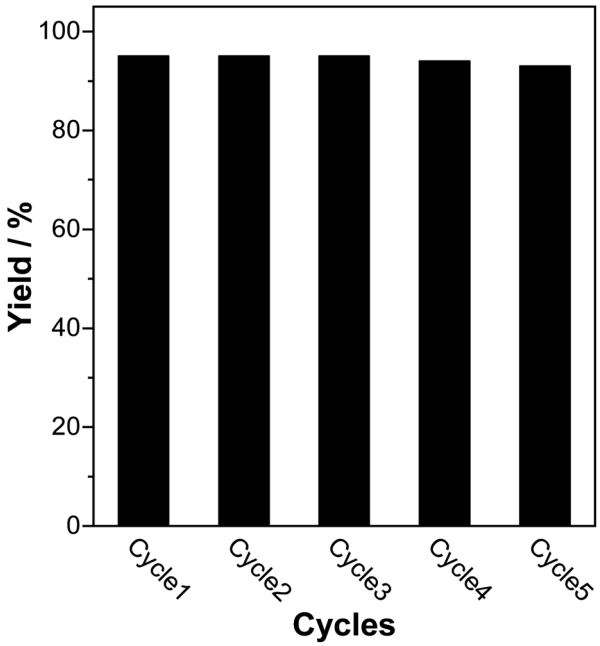

Fig. 8 Recyclability of the SMCNC catalyst for the synthesis of product **3a**.

2.4. Reaction mechanism

2.4.1. Knoevenagel reaction. Fig. 7a depicts the proposed reaction mechanism for access to α,β-unsaturated nitrile derivatives based on the literature.[6,79] The key factor for the proposed mechanism is that acidic sulfonic sites enable the Knoevenagel coupling by polarizing the carbonyl group of benzaldehyde, where it can coordinate with oxygen and further be attacked by the pronucleophile-like malononitrile or ethyl cyanoacetate. Afterward, a water molecule was eliminated to yield the α,β-unsaturated product.

2.4.2. Thorpe–Ziegler reaction. According to the previous findings and relying on the literature reports,[22,80,81] the following reaction mechanism shown in Fig. 7b was suggested for the synthesis of thienopyridine products in the presence of the MSCNC catalyst as a cascade reaction. Because of their acidic properties, the MSCNCs could act as a Brønsted-acid in various phases, facilitating the alkylation reaction of the thiol group with the halogenated carbonyl compound. The nucleophilic addition of CH_2 hydrogen into the nitrile (CN) group undergoes intramolecular tautomerization of the imine intermediate to deliver the thienopyridine product.

2.5. Catalyst recycling

The catalyst reusability was investigated by repetition of the reaction under the optimized conditions of water as a solvent at room temperature for 30 min, and in the presence of a 10%

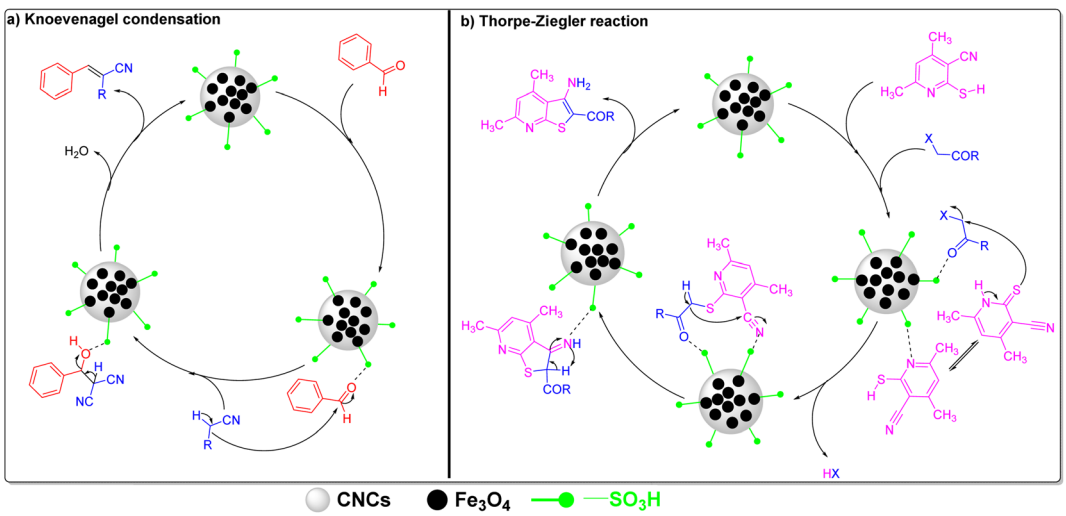

Fig. 7 Mechanistic routes of (a) Knoevenagel condensation and (b) Thorpe–Ziegler reaction over SMCNCs.

Table 3 Comparison of the performance of the SMCNCs with other reported catalysts

Entry	Catalyst	Time (min)	Conditions	Yield (%)	Ref.
1	$Ag@TiO_2$	60	EtOH, 65 °C	95	6
2	Br_3-TBA-Fe_3O_4	60	H_2O, reflux	91	82
3	Pd@g-C_3N_4	180	Toluene, 65 °C	88.3	83
4	Alum-Cs_2CO_3	180	H_2O, reflux	94	84
5	Nylon 6-NH	30	Cyclohexane, 80 °C	95	79
6	Fe_3O_4-PIL	10	H_2O, ultrasound	92	85
7	Sulfonated-g-C_3N_4	30	EtOH, 50 °C	90	26
8	Fe_3O_4@EDTA@GO	60	THF, 50 °C	55	86
9	SMCNC	30	H_2O, r.t	97	This work

catalyst load. After completing the reaction, the SMCNCs were separated using a neodymium magnet and rinsed in ethyl acetate, ethanol, and acidified distilled water to remove any adsorbed contaminations. The recovered catalyst was dried for 12 h at 80 °C before being reused in the next cycle. As illustrated in Fig. 8, the catalyst could be recycled and reused 5 times without a significant decrease in the catalytic efficiency. These findings revealed that the SMCNCs demonstrated exceptional reusability and substantial performance for the Knoevenagel reaction, which is a promising factor in industrial work. Comparing the FTIR (Fig. S3†), XRD (Fig. S4†), and XPS S 2p (Fig. S5†) spectra of the recovered SMCNCs with the corresponding spectra of the as-prepared SMCNCs illustrates that there are no deviations in the chemical composition or the crystalline structures of the recycled SMCNCs.

2.6. Comparison with the reported catalysts for Knoevenagel condensation

Table 3 illustrates the comparison between the catalytic activity of our SMCNC catalyst and other reported catalysts for the synthesis of α,β-unsaturated esters and nitriles through Knoevenagel condensation. Our results show that the SMCNCs have the advantages of green synthetic procedures, a clean reaction profile, a short reaction time, and high yields. The SMCNCs were easily isolated from the reaction mixture, and the Knoevenagel reaction can be catalyzed by the SMCNCs using a green approach, without applying hazardous reagents or harsh conditions.

3. Experimental

3.1. Materials

Microcrystalline cellulose (MCC, 51 μm), ferric chloride hexahydrate ($FeCl_3 \cdot 6H_2O$, 97%), ferrous chloride tetrahydrate ($FeCl_2 \cdot 4H_2O$, 98%), hydrochloric acid (37%), urea (99%), chlorosulfonic acid (99%), piperidine (99%), benzaldehyde and its derivatives (99%), malononitrile (99%), ethyl cyanoacetate (99%), ethyl chloroacetate (99%), chloroacetone (99%) and chloroacetamide (99%) were purchased from Sigma-Aldrich.

3.2. Synthesis of SMCNCs

In a Teflon-lined container (200 mL), 2 g of MCC, 1.2 g of $FeCl_2 \cdot 4H_2O$, 1.6 g of $FeCl_3 \cdot 6H_2O$, and 25 g of urea were vigorously stirred in 100 mL of HCl (4 M) for 20 min. Then, the Teflon container was sealed and transferred into a stainless-steel autoclave, which was heated at 180 °C for 20 h. The developed MCNCs were collected using a neodymium magnet and soaked in NaOH (0.01 M) for three hours. The collected MCNCs were washed three times through sonication in ultrapure water for 5 min and dried at 60 °C. For the synthesis of SMCNCs, 0.5 g of NaOH-treated MCNCs were dispersed in 100 mL of DMF and then 240 μL of CSA (98%, Sigma-Aldrich) was added to the system under gentle stirring (50 rpm) for 1 h at room temperature.[43,51,52]

3.3. The general method for Knoevenagel condensation

In a representative experimental procedure, benzaldehyde **1a** (0.21 gm, 2 mmol) was transferred into a 25 mL reaction flask charged with malononitrile **2a** (0.20 gm, 3 mmol), 5 mL of water and SMCNCs (10% wt.). The reaction was accomplished under stirring conditions at ambient temperature for the mentioned time. The reaction completion was followed using thin-layer chromatography (TLC). After reaction completion, the SMCNCs were collected using a neodymium magnet, and the reaction product was collected after precipitation. The reaction yield was calculated using eqn (2). The SMCNC catalyst can be easily reactivated by washing it in ethyl acetate, ethanol, HCl (0.1 mM) and in ultrapure water, and finally drying at 80 °C.

$$\text{Yield}(\%) = \frac{\text{actual yield}}{\text{theortical yield}} \times 100 \quad (2)$$

3.4. The general method for Thorpe–Ziegler condensation

In a typical experimental procedure, compound **4** (0.33 gm, 2 mmol) was transferred to a 25 mL reaction vessel charged with α-halogenated carbonyl compound **5** (2.5 mmol), ethanol (5 mL), and SMCNCs (10% wt.). The reaction was refluxed in an oil bath under stirring for the appropriate time. The reaction completion was followed using TLC. After the completion of the reaction, the SMCNCs were collected using a neodymium magnet, and the reaction product was collected after precipitation. The reaction yield was calculated using eqn (2).

3.5. Characterization

The zeta potential, hydrodynamic diameter, crystallinity, chemical constituents, and morphology of the SMCNCs were studied. Using a PALS zeta analyzer (Nano Brook, Brookhaven,

U.S.A.), the zeta potential and hydrodynamic diameter of the SMCNCs (0.2 g in 10 mL of deionized water) were calculated from the mean of ten measurements. The XRD diffraction spectra were calculated using a Panalytical X'pert Pro diffractometer equipped with Cu Kα radiation with a 1.5419 Å wavelength at 40 kV and 40 mA. The 2θ range was between 10° and 68°, and the resolution was 2°/min with a step size of 0.02°. The background was collected from a clean silicon wafer substrate, and then the samples were transferred onto a silicon wafer to collect their XRD spectra. The background correction was performed by subtracting the background spectrum from the samples' spectra. Peak polarization and deconvolution were performed using the PeakFit software. Using Bruker Tensor 37, the FTIR spectra were collected at a resolution of 4 cm^{-1} and 1024 scan cycles while applying Attenuated Total Reflection (ATR) mode using a single-reflection ATR accessory equipped with a ZnSe crystal. The XPS spectra were collected using a Kratos Axis Supra (Shimadzu Group Company, Japan) with monochromatic Al Kα radiation. The CasaXPS software was utilized for the spectra deconvolution. A Thermo-Fischer scientific Talos F200X Field emission transmission electron microscope (S/TEM) equipped with a super-X four-quadrant energy dispersive X-ray spectrometer (EDS) was utilized for investigating the morphology, crystallinity, and elemental mapping of the samples. A thermogravimetric analyzer (Q50, USA) was used for the thermal gravimetrical analysis (TGA) and differential thermal analysis (DTA), and the measurements were carried out under a 50 mL min^{-1} nitrogen flow with a heating rate of 10 °C min^{-1} to approach the temperature of 800 °C. The NMR spectra of the Knoevenagel and Thorpe–Ziegler products were collected using an INOVA-500 MHz instrument (Varian, Palo Alto, CA, USA), and the internal standard of trimethylsilyl propanoic acid (TSP) was used.

4. Conclusions

A new catalytic methodology for Knoevenagel condensation and Thorpe–Ziegler cyclization was established utilizing a heterogeneous SMCNC catalyst. The catalyst was synthesized in two steps, which were hydrothermal production of MCNCs followed by $ClSO_3H$ post-sulfonation. To determine the optimal conditions for both reactions, many different conditions were attempted, and these optimal conditions were employed for a broad scope of aldehydes and active methylene substrates for Knoevenagel condensation and Thorpe–Ziegler cyclization. The catalyst was efficient for 5 cycles of reaction without a significant decrease in the isolated yield. The presence of SO_3H components promoted the reactions, while the presence of Fe_3O_4 facilitated the isolation of the catalyst from the reaction medium without tiresome procedures. Hence, the catalyst affords a facile green synthetic strategy with a clean reaction profile and high yields.

Data availability

All the data are available in this manuscript and ESI.†

Author contributions

Mostafa Sayed: conceptualization; data curation; formal analysis; investigation; methodology; roles/writing – original draft; writing – review & editing & Abdelreheem Abdelfatah Saddik: conceptualization; data curation; formal analysis; investigation & Adel M. Kamal El-Dean: supervision; validation & Pedram Fatehi: funding acquisition; supervision; validation & Ahmed I. A. Soliman: conceptualization; data curation; formal analysis; investigation; methodology; roles/writing – original draft; writing – review & editing, supervision.

Conflicts of interest

There are no conflicts of interest to be declared.

Acknowledgements

MS is grateful for financial support from the CAS-TWAS Fellowship. AIAS acknowledges Assiut University and Zhejiang University for financial support.

References

1 L. Liu and A. Corma, *Chem. Rev.*, 2018, **118**, 4981–5079.
2 M. F. I. Al-Hussein and M. S. S. Adam, *Appl. Organomet. Chem.*, 2020, **34**, e5598.
3 B. Changmai, G. Pathak, J. M. H. Anal and L. Rokhum, *Mini-Rev. Org. Chem.*, 2020, **17**, 740–753.
4 A. Mukhtar, S. Saqib, H. Lin, M. U. Hassan Shah, S. Ullah, M. Younas, M. Rezakazemi, M. Ibrahim, A. Mahmood, S. Asif and A. Bokhari, *Renewable Sustainable Energy Rev.*, 2022, **157**, 112012.
5 A. Ying, L. Wang, F. Qiu, H. Hu and J. Yang, *C. R. Chim.*, 2015, **18**, 223–232.
6 M. Sayed, Z. Shi, F. Gholami, P. Fatehi and A. I. A. Soliman, *ACS Omega*, 2022, **7**, 32393–32400.
7 D. Elhamifar, S. Kazempoor and B. Karimi, *Catal. Sci. Technol.*, 2016, **6**, 4318–4326.
8 J. Huang, S. Ding, W. Xiao, Y. Peng, S. Deng and N. Zhang, *Catal. Lett.*, 2015, **145**, 1000–1007.
9 G. B. B. Varadwaj, S. Rana and K. M. Parida, *Dalton Trans.*, 2013, **42**, 5122–5129.
10 Z. Wu, Z. He, Y. Xu, J. Wang, X. Lu, Q. Xia and D. Zhou, *J. Porous Mater.*, 2021, **28**, 1041–1048.
11 J.-P. Grass, K. Klühspies, B. Reiprich, W. Schwieger and A. Inayat, *Catalysts*, 2021, **11**, 474.
12 G.-Q. Huang, J. Chen, Y.-L. Huang, K. Wu, D. Luo, J.-K. Jin, J. Zheng, S.-H. Xu and W. Lu, *Inorg. Chem.*, 2022, **61**, 8339–8348.
13 J. Qiao, B. Zhang, L. Zhang and Y. Liu, *J. Mater. Chem. A*, 2022, **10**, 17773–17781.
14 S. Johari, M. R. Johan and N. G. Khaligh, *Org. Biomol. Chem.*, 2022, **20**, 2164–2186.
15 Y. Kumar, J. Shabir, P. Gupta and L. S. Kumar, *Catal. Lett.*, 2022, **152**, 1506–1516.

16 A. Brzęczek-Szafran, M. Gwóźdź, A. Kolanowska, M. Krzywiecki, P. Latos and A. Chrobok, *React. Chem. Eng.*, 2021, **6**, 1246–1253.
17 N. Zengin, H. Burhan, A. Şavk, H. Göksu and F. Şen, *Sci. Rep.*, 2020, **10**, 12758.
18 M. Ahmed, M. Sayed, A. F. Saber, R. Hassanien, A. M. Kamal El-Dean and M. S. Tolba, *Polycyclic Aromat. Compd.*, 2022, **42**(6), 3079–3088.
19 M. Sayed, O. Younis, R. Hassanien, M. Ahmed, A. A. K. Mohammed, A. M. Kamal and O. Tsutsumi, *J. Photochem. Photobiol., A*, 2019, **383**, 111969.
20 A. A. Saddik, A. M. Kamal El-Dean, W. A. El-Said, K. M. Hassan and M. S. Abbady, *J. Heterocycl. Chem.*, 2018, **55**, 2111–2122.
21 A. A. Saddik, A. M. Kamal El-Dean, G. H. El-Sokary, K. M. Hassan, M. S. Abbady, I. A. Ismail and S. H. Saber, *J. Chin. Chem. Soc.*, 2017, **64**, 87–93.
22 Y. A. Attia and S. H. Abdel-Hafez, *Res. Chem. Intermed.*, 2021, **47**, 3719–3732.
23 L. Shiri, H. Narimani and M. Kazemi, *Appl. Organomet. Chem.*, 2018, **32**, e3927.
24 M. B. Gawande, A. K. Rathi, I. D. Nogueira, R. S. Varma and P. S. Branco, *Green Chem.*, 2013, **15**, 1895–1899.
25 F. H. Norouzi, N. Foroughifar, A. Khajeh-Amiri and H. Pasdar, *RSC Adv.*, 2021, **11**, 29948–29959.
26 P. Choudhary, A. Sen, A. Kumar, S. Dhingra, C. M. Nagaraja and V. Krishnan, *Mater. Chem. Front.*, 2021, **5**, 6265–6278.
27 T. Chhabra, P. Dwivedi and V. Krishnan, *Green Chem.*, 2022, **24**, 898–910.
28 F. Lashkari, R. Badri and E. Tahanpesar, *Iran. J. Sci. Technol. Trans. A: Sci.*, 2020, **44**, 1357–1367.
29 A. Barzkar and A. S. Beni, *RSC Adv.*, 2020, **10**, 41703–41712.
30 K. Debnath, K. Singha and A. Pramanik, *RSC Adv.*, 2015, **5**, 31866–31877.
31 S. Kamel and T. A. Khattab, *Cellulose*, 2021, **28**, 4545–4574.
32 K. Shelke, S. Sapkal, K. Niralwad, B. Shingate and M. Shingare, *Open Chem.*, 2010, **8**, 12–18.
33 Y. Shen, C. Yuan, X. Zhu, Q. Chen, S. Lu and H. Xie, *Green Chem.*, 2021, **23**, 9922–9934.
34 Z. Ghasemi, A. H. Amale, S. Azizi, S. Valizadeh and J. Soleymani, *RSC Adv.*, 2021, **11**, 36958–36964.
35 B. Kumar, M. S. Reddy, K. D. Dwivedi, A. Dahiya, J. N. Babu and L. R. Chowhan, *Appl. Organomet. Chem.*, 2022, **36**, 1–10.
36 M. H. Beyki and M. H. Ghasemi, *Int. J. Biol. Macromol.*, 2018, **113**, 711–718.
37 M. Gericke, J. Trygg and P. Fardim, *Chem. Rev.*, 2013, **113**, 4812–4836.
38 Y. Habibi, L. A. Lucia and O. J. Rojas, *Chem. Rev.*, 2010, **110**, 3479–3500.
39 Y. Shen, C. Yuan, X. Zhu, Q. Chen, S. Lu and H. Xie, *Green Chem.*, 2021, **23**, 9922–9934.
40 H. Ma, L. Zou, L. Mi, H. Pan, Y. Qiao, N. Li and J. Teng, *ChemistrySelect*, 2018, **3**, 11110–11117.
41 Y. Jiao, C. Wan, W. Bao, H. Gao, D. Liang and J. Li, *Carbohydr. Polym.*, 2018, **189**, 371–378.
42 M. S. Islam, L. Chen, J. Sisler and K. C. Tam, *J. Mater. Chem. B*, 2018, **6**, 864–883.
43 J. Luo, N. Semenikhin, H. Chang, R. J. Moon and S. Kumar, *Carbohydr. Polym.*, 2018, **181**, 247–255.
44 M. Cheng, Z. Qin, Y. Chen, S. Hu, Z. Ren and M. Zhu, *ACS Sustain. Chem. Eng.*, 2017, **5**, 4656–4664.
45 F. Fu, M. Xu, H. Wang, Y. Wang, H. Ge and J. Zhou, *ACS Sustain. Chem. Eng.*, 2015, **3**, 1510–1517.
46 I. Martínez-Mera, M. E. Espinosa-Pesqueira, R. Pérez-Hernández and J. Arenas-Alatorre, *Mater. Lett.*, 2007, **61**, 4447–4451.
47 C.-C. Lin and C.-Y. Lee, *Mater. Chem. Phys.*, 2020, **240**, 122049.
48 J. Wei, Y. Zhou, Y. Lv, J. Wang, C. Jia, J. Liu, X. Zhang, J. Sun and Z. Shao, *ACS Sustain. Chem. Eng.*, 2019, **7**, 12887–12896.
49 K. N. M. Amin, A. Hosseinmardi, D. J. Martin and P. K. Annamalai, *J. Bioresour. Bioprod.*, 2022, **7**, 99–108.
50 P. Liu, X. Guo, F. Nan, Y. Duan and J. Zhang, *ACS Appl. Mater. Interfaces*, 2017, **9**, 3085–3092.
51 B. Pingrey and Y.-L. Hsieh, *Biomacromolecules*, 2022, **23**, 1269–1277.
52 A. De Nino, M. A. Tallarida, V. Algieri, F. Olivito, P. Costanzo, G. De Filpo and L. Maiuolo, *Appl. Sci.*, 2020, **10**, 8155.
53 J. Sun, L. Cui, Y. Gao, Y. He, H. Liu and Z. Huang, *Carbohydr. Polym.*, 2021, **251**, 117004.
54 Z. Guo, R. Yang, F. Yang, L. Sun, Y. Li and J. Xu, *Int. J. Biol. Macromol.*, 2021, **184**, 68–78.
55 W. Yang, H. Tian, J. Liao, Y. Wang, L. Liu, L. Zhang and A. Lu, *Appl. Surf. Sci.*, 2020, **507**, 145092.
56 A. I. A. Soliman, Y. Tu, T. Utsunomiya, T. Ichii and H. Sugimura, *Langmuir*, 2017, **33**, 10829–10837.
57 S. Thota, V. Somisetti, S. Kulkarni, J. Kumar, R. Nagarajan and R. Mosurkal, *Cellulose*, 2020, **27**, 11–24.
58 J. Liu, D. Liu, S. Liu, Z. Li, X. Wei, S. Lin and M. Guo, *Energy Environ. Mater.*, 2020, **3**, 209–215.
59 M. Cheng, Z. Qin, Y. Chen, J. Liu and Z. Ren, *Cellulose*, 2017, **24**, 3243–3254.
60 M. Usman, J. M. Byrne, A. Chaudhary, S. Orsetti, K. Hanna, C. Ruby, A. Kappler and S. B. Haderlein, *Chem. Rev.*, 2018, **118**, 3251–3304.
61 F. D'Acierno, W. Y. Hamad, C. A. Michal and M. J. Maclachlan, *Biomacromolecules*, 2020, **21**, 3374–3386.
62 N. Li, H. Ke, T. Wang and S. Xia, *J. Pet. Sci. Eng.*, 2022, **211**, 110112.
63 J. O. Zoppe, L. S. Johansson and J. Seppälä, *Carbohydr. Polym.*, 2015, **126**, 23–31.
64 Y. Guo, Y. Zhang, D. Zheng, M. Li and J. Yue, *Int. J. Biol. Macromol.*, 2020, **163**, 927–933.
65 F. Nan, S. Nagarajan, Y. Chen, P. Liu, Y. Duan, Y. Men and J. Zhang, *ACS Sustain. Chem. Eng.*, 2017, **5**, 8951–8958.
66 J. Zhao, M. Deng, S. Li, Z. Guan, Y. Xia, J. Yang and X. Lin, *Carbohydr. Polym.*, 2022, **278**, 118946.
67 S. Gan, S. Zakaria and S. N. Syed Jaafar, *Carbohydr. Polym.*, 2017, **172**, 284–293.
68 Y. Wei, M. Zhou, A. Yao and P. Zhu, *Appl. Sci.*, 2020, **10**, 1977.
69 S. Gan, S. Zakaria, K. M. Salleh, N. I. S. Anuar, S. Moosavi and R. S. Chen, *Int. J. Biol. Macromol.*, 2020, **158**, 552–561.
70 F. Fu, Q. Yang, J. Zhou, H. Hu, B. Jia and L. Zhang, *ACS Sustain. Chem. Eng.*, 2014, **2**, 2604–2612.

71 J. F. Gu, C. Chen, Z. H. Zheng, J. Hang, W. Sang, J. C. Wang, Y. Yuan, S. Chaemchuen and F. Verpoort, *J. Catal.*, 2023, **417**, 202–212.
72 V. S. Marakatti, J. Klimeš, P. Kasinathan, K. Sorathia, D. P. Tew and E. M. Gaigneaux, *Catal. Sci. Technol.*, 2021, **11**, 1345–1357.
73 F. Cataldo, *Eur. Chem. Bull.*, 2015, **4**, 92–97.
74 G. Li, B. Wang and D. E. Resasco, *Surf. Sci. Rep.*, 2021, **76**, 100541.
75 P. J. Dyson and P. G. Jessop, *Catal. Sci. Technol.*, 2016, **6**, 3302–3316.
76 R. Devi, P. Begum, P. Bharali and R. C. Deka, *ACS Omega*, 2018, **3**, 7086–7095.
77 V. S. Marakatti, J. Klimeš, P. Kasinathan, K. Sorathia, D. P. Tew and E. M. Gaigneaux, *Catal. Sci. Technol.*, 2021, **11**, 1345–1357.
78 C. Reichardt and T. Welton, in *Solvents and Solvent Effects in Organic Chemistry*, Wiley-VCH Verlag GmbH & Co. KGaA, Weinheim, Germany, 2010, pp. 7–64.
79 Z. Yan, Y. Liu, W. Wang and D. Wang, *ACS Omega*, 2022, **7**, 33186–33191.
80 M. Esmaeilpour, J. Javidi and M. Divar, *J. Magn. Magn. Mater.*, 2017, **423**, 232–240.
81 N. Mohammadian and B. Akhlaghinia, *Res. Chem. Intermed.*, 2019, **45**, 4737–4756.
82 L. Shiri, S. Rahmati, Z. Ramezani Nejad and M. Kazemi, *Appl. Organomet. Chem.*, 2017, **31**, e3687.
83 H. Wang, Y. Wang, Y. Guo, X.-K. Ren, L. Wu, L. Liu, Z. Shi and Y. Wang, *Catal. Today*, 2019, **330**, 124–134.
84 A. K. Taduri and B. R. Devi, *Asian J. Chem.*, 2014, **26**, 1938–1942.
85 N. Kakesh, S. Sayyahi and R. Badri, *C. R. Chim.*, 2018, **21**, 1023–1028.
86 H. M. A. Hassan, R. F. M. Elshaarawy, S. K. Dey, I. Simon and C. Janiak, *Catal. Lett.*, 2017, **147**, 1998–2005.